Tellus (1989), *41A*, 371–384

An examination of midlatitude power spectra: evidence for standing variance and the signature of El Niño

By ANTHONY R. HANSEN[1], ALFONSO SUTERA[2] and DAVID E. VENNE[1],
[1]*Meteorology Research Center, Control Data Corporation, Minneapolis, MN 55440;*
[2]*Department of Geology and Geophysics, Yale University, New Haven, CT 06511, USA*

(Manuscript received 14 June 1988; in final form 11 October 1988)

ABSTRACT

Low-frequency variability in the midlatitude winter circulation is investigated by computation of power spectra from 16 winters of Northern Hemisphere (NH) NMC data and 4 winters of Southern Hemisphere (SH) ECMWF data. Different techniques of partitioning the variance are compared. The results for the two hemispheres are similar in that a substantial standing variance with periods of 10 days and longer is found in both hemispheres. In the NH, this strong standing variance spans wavenumbers 2 through 4, while in the SH, it is quite prominent at wavenumber 3. The standing variance corresponds to wavenumbers exhibiting bimodal probability density distributions. Interhemispheric differences center around much stronger westward-traveling ultralong wave variance in the NH but stronger eastward traveling intermediate wavenumber variance in the SH. These interhemispheric differences in the traveling variance are likely an effect of the presence or absence of topographic forcing, as suggested by earlier GCM experiments. This implies that the rôle of the stationary topographic forcing is more significant for the traveling waves than for the standing waves. In addition, composite power spectra for El Niño, anti-El Niño and non-El Niño NH winters were constructed. The results indicate that the warm equatorial sea surface temperature (SST) anomalies of El Niño are accompanied by a strong composite spectral peak at wavenumber 7 with 5-day period in the midlatitude power spectra. Examination of individual winters reveals that this apparent difference does appear fairly consistently in all El Niño winters, but some control and anti-El Niño winters exhibit similar peaks. The most consistent difference between power spectra composed on the basis of SST anomalies is relatively stronger standing variance in the anti-El Niño composite and weak standing variance in the El Niño composite.

1. Introduction

Traditionally, studies of the general circulation have focused on the balance requirements of the time averaged state of the atmosphere (e.g., Lorenz, 1967). Recently however, much attention has been focused on the slowly varying components of the circulation (e.g., Wallace and Blackman, 1983). In general, this includes all circulation features with time-scales longer than that of synoptic scale cyclones. Study in this area might crudely be separated between studies of interannual (or interseasonal) variability and intraseasonal variability. In either case, fundamental questions arise concerning the physical nature and origin of the observed variability. The importance of boundary forcing, internal dynamics and the potential coupling of these sources of long period variability are important issues.

In the present study, attention is focused on the midlatitude winter circulation in both the Northern Hemisphere (NH) and Southern Hemisphere (SH) by means of power spectrum analysis. Numerous studies of large-scale, wavenumber-frequency power spectra computed from observations and models may be found in the literature (e.g., Pratt and Wallace, 1976; Fraedrich and Böttger, 1978; Hayashi and Golder, 1977, 1983; Speth and Madden, 1983; Mechoso et al., 1987;

see Hayashi, 1982 for a thorough review). The advantage of this tool is that it separates atmospheric variability by space and time scale, thus elucidating the regions of wavenumber-frequency space characterizing the variance. A principal drawback is that it presents continuous atmospheric spectra in terms of discrete wavenumber and frequency components. One of the motivations behind wavenumber-frequency analysis has been the desire to partition the variance associated with atmospheric fluctuations into eastward propagating components, westward propagating components, standing components and noise introduced by errors in the observations (Deland, 1972). However, none of the available techniques are capable of a complete partitioning of the variance without numerous, restrictive assumptions (Deland, 1972; Tsay, 1974; Pratt, 1976; Hayashi, 1977, 1979; Schafer, 1979; etc.). Nonetheless, by intercomparing the results obtained from different methods and being aware of the limitations of each, bounds may be put on the various components of the variance that provide useful information for further investigation and understanding of the general circulation.

In the present study, techniques developed by Hayashi (1979), Schafer (1979), and an earlier technique of Hayashi (1971) used by Fraedrich and Böttger (1978) will be compared to identify principal regions of strong variance in wavenumber-frequency space. Results for both the NH and SH are computed and compared. Due to interhemispheric differences in stationary forcing, some limited conclusions can be drawn concerning the rôle of topographic forcing, for example, in the low wavenumber, low frequency part of the spectrum.

Of particular interest is an area that has received relatively little attention in the literature; that is, the relative strength of the standing variance in midlatitudes. This topic has relevance to the interpretation of recent observational results on low frequency variability which indicate bimodality in the combined amplitudes of zonal wavenumbers 2, 3 and 4 (Sutera, 1986; Hansen, 1986; Hansen and Sutera, 1986) in the NH and at wavenumber 3 in the SH (Hansen and Sutera, 1988). One theoretical framework for explaining these observations involves a nonlinear mechanism which predicts standing variance near these wavenumbers (e.g., Benzi et al., 1986a, b). The emerging picture from this and other studies is that topographic forcing may not be fundamentally important in explaining the standing variance or bimodality. On the other hand, topography may play an important rôle in effecting the traveling variance.

A separate issue related to interannual or interseasonal variability centers around the question of whether long period changes in boundary conditions, such as the tropical Pacific sea surface temperature (SST) anomalies of El Niño (Rasmussen and Carpenter, 1982) can influence the circulation in midlatitudes in a consistent, predictable way. Recent GCM studies (Mechoso et al., 1987) have suggested that warm equatorial Pacific SST anomalies associated with the El Niño/Southern Oscillation may act to enhance high frequency, intermediate scale wave activity (wave 6, 4 day period) in NH midlatitudes. We explore whether any differences in power spectra may be present in observations composited between El Niño winters, anti-El Niño winters (cold SST anomalies in the eastern tropical Pacific) and control winters not exhibiting tropical SST anomalies of either sign.

2. Spectral analysis techniques

As discussed by Hayashi (1979, 1982), the observed total variance T in a given wavenumber and frequency interval is composed of standing variance (S), westward (W) and eastward (E) traveling variance and noise (N) introduced by errors in the data and the approximate nature of the spectral estimates. Symbolically, $T = S + E + W + N$. Assumptions are necessary to perform a partitioning of this variance and no technique is capable of performing a complete partitioning without resort to severe assumptions.

A study of NH midlatitudes by Fraedrich and Böttger (1978) indicated a spectral peak in the standing variance at wavenumber 3 and 20 day period, along with peaks in the traveling variance for wavenumbers 5–6 and 7–8 near 8 and 5 day periods, respectively. However, subsequent refinements in power spectral techniques indicated that the approach used by Fraedrich and Böttger (i.e., that of Hayashi, 1971) will overestimate (possibly severely) the standing variance. Traveling variance in their study was assumed to be represented by the cosine–sine quadrature spectrum for each wavenumber with the remainder of the total variance assigned to the standing waves. However, the contribution of the noise to the total variance is included with this residual standing variance. The noise can make significant contributions to the total variance, particularly at the lowest frequencies resolved by a lag correlation method (e.g., Schafer, 1979).

Hayashi (1977, 1979, 1982) has developed an improved technique for partitioning the total variance between standing and traveling parts. A progressive–retrogressive coherence is computed (an extension of the usual cosine–sine coherence), and it is assumed that:

(1) A time series can be partitioned between traveling and standing components which are incoherent with each other. This assumes that the standing and traveling waves arise from different physical causes.

(2) The standing component represents progressive and retrogressive components of the same magnitude and coherent with each other.

(3) The traveling components are defined as the progressive and retrogressive components that are incoherent with each other.

Symbolically, this partitioning of the total variance may be expressed as $T = E_H + W_H + S_H$, where the H subscript refers to the Hayashi estimate of the components of the variance. In this case, part of the traveling variance is due to random noise that contributes equally to the progressive and retrogressive components of the variance. That is, $E_H = E + \frac{1}{2}N$ and $W_H = W + \frac{1}{2}N$. The result of this partitioning is illustrated in Fig. 1a (adapted from Hayashi, 1979, 1982). Thus, the traveling variance will be overestimated (perhaps severely) at low frequencies when observational data is used.

An alternate approach can be taken to partition the wave components and noise components of the variance by making a different set of assumptions (Schafer, 1979; Hayashi, 1979).

(1) The cosine and sine components of the wave disturbances are coherent with one another (i.e., the components of the traveling and standing variance arise from the same source), and

(2) The noise is represented by cosine and sine components that are of equal amplitude and incoherent with one another.

Symbolically, the Schafer partitioning (denoted by the S subscript) may be written as $T = E_S + W_S + N_S$. The eastward and westward traveling variance isolated as distinct from the noise by this technique will contain both the actual traveling variance plus the standing variance as illustrated in Fig. 1b. That is, $E_S = E + \frac{1}{2}S$ and $W_S = W + \frac{1}{2}S$. Thus, the strength of the traveling variance may also be overestimated by Schafer's technique.

An upper bound for the standing variance may be obtained from the equal amplitude parts of the coherent variance. That is $(S_S)_{\text{upperbound}} = 2 * \min(E_S, W_S)$. A pure standing wave is diagnosed by the Schafer technique as equal parts of

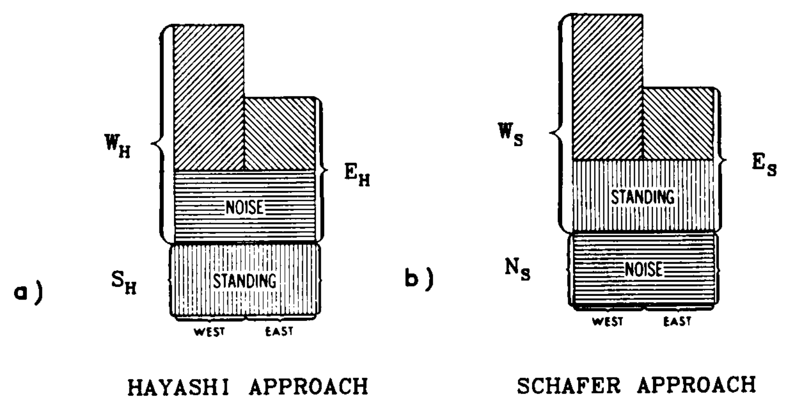

Fig. 1. Schematic representation of the partitioning of variance between eastward traveling (*E*), westward traveling (*W*), standing (*S*) and noise (*N*) components for (a) the Hayashi (1979) approach and (b) the Schafer (1979) approach (adapted from Hayashi, 1979, 1982).

eastward and westward propagating variance. Thus, if the eastward and westward variance are of comparable amplitude, we have a necessary condition for the existence of a large standing component. It is not a sufficient condition, however, because the flow could in principle shift between pure eastward or pure westward propagation that is coherent. (This can be verified with synthetic data). On the other hand, if the eastward and westward variance are widely different in magnitude, we would suspect that the standing variance was relatively small.

It should be noted that in small samples both the Hayashi and Schafer techniques will tend to overestimate the coherence between eastward and westward traveling variance and hence overestimate the standing variance.

Since all three methods discussed above are describing the same variance, comparison of the results from all three can lead to some insight. We must keep in mind, however, that the assumptions made in the different approaches are not compatible so they can't be compared directly or quantitatively.

3. Approach and data

We will consider each of the 3 techniques discussed in the previous section to estimate power spectra of the NH midlatitudes from 16 winters of National Meteorological Center (NMC) 500 mb geopotential height data (1964–65 to 1979–80) and of the SH midlatitudes from 4 SH winters of European Centre for Medium Range Weather Forecasts (ECMWF) 500 mb geopotential height data (1980 to 1983). The NH winter season is taken to be the 120-day period from 16 November–15 March of each year and the SH winter is considered the 120 day period from 18 May to 14 September. The spectral estimates are computed using a Tukey window with a maximum lag of 21 days. The data are daily (0000 GMT) in both datasets. Results for the resolved periods from 40 days to 2 days will be presented. The NMC data were interpolated from the NMC octagon grid onto a 5° latitude-longitude grid. The ECMWF data are on a 5.625° latitude-longitude grid. Zonal wavenumbers 1 through 10 are considered. We depart from previous studies in that we will present results for geopotential heights averaged across the 40° to 60° latitude zone in each hemisphere. In this way, the average conditions for midlatitudes are presented succinctly for easy comparison. Changes in the spectra that occur as a function of latitude will be noted where appropriate.

4. Intraseasonal midlatitude variance

4.1. Northern hemisphere results

In this part of the study, emphasis is placed on the low frequency, low wavenumber part of the spectrum. Thus, we follow Fraedrich and Böttger (1978) in presenting the spectral density results on log–log diagrams. In order to make equal areas on these diagrams represent equal variance, the spectral densities are normalized by their wavenumber and frequency. This procedure will tend to emphasize spectral peaks in otherwise red spectra.

The results for the Hayashi approach are presented in Fig. 2. For the propagating variance, well known spectral peaks occur for the westward propagating ultralong waves near 20 day period, (e.g., Speth and Madden, 1983) and for the eastward propagating waves near wavenumber 6 and 7 at roughly 5-day period (Fig. 2a). Note that the ultralong wave peak occurs at wavenumber 2 instead of wavenumber 1 as, for example, in Speth and Madden (1983) because of the noted normalization. The westward propagating ultralong wave variance is relatively more prominent at higher latitudes (not shown). The double maxima in eastward traveling variance at higher wavenumbers are similar to those discussed by Fraedrich and Böttger (1978). The Hayashi estimate of the standing variance (Fig. 2b) indicates greatest power at wavenumbers 2 through 4 and periods longer than 10 days. The standing variance in this diagram peaks at wavenumbers 3 and 4. The largest standing variance in Fig. 2b is at wavenumber 4, 40 day period. However, at individual latitude circles the peak standing variance shifts from wavenumber 4 to wavenumber 3 and finally to wavenumber 2 as latitude increases poleward.

The present standing variance result is qualitatively in agreement with that of Fraedrich and Böttger (1978) but the level of the standing variance is substantially less in the present result.

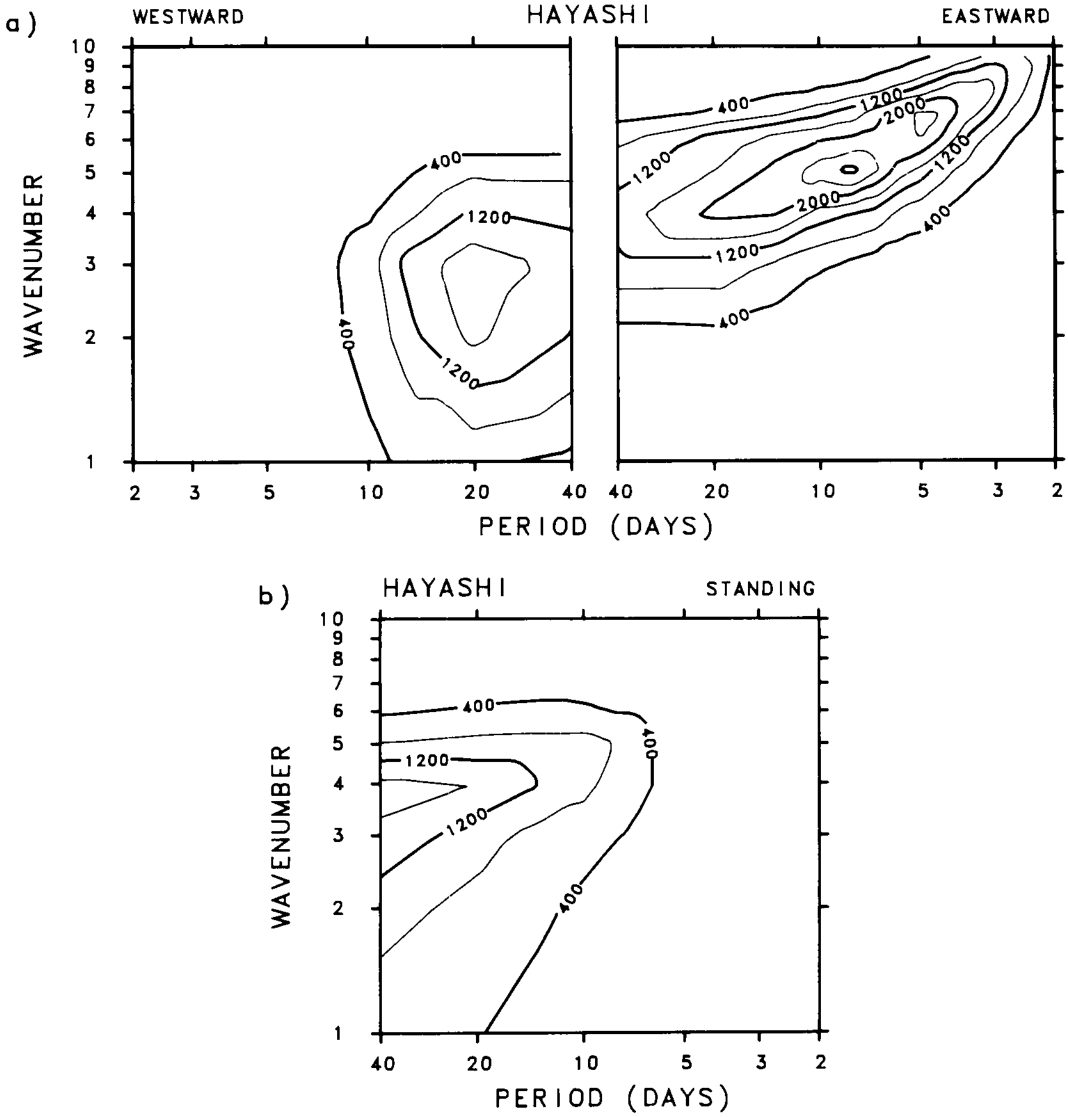

Fig. 2. Power spectral density for the NH winter 500 mb geopotential height averaged between 40°N and 60°N determined by the Hayashi (1979) technique (a) for the westward and eastward traveling variance and (b) for the standing variance. Units are m^2, see text for discussion of normalization used in this and subsequent diagrams. The contour interval in this and subsequent figures is 400 m^2 except where noted.

This is due to the inclusion of the noise component with the standing variance estimate in Fraedrich and Böttger's technique as we will show shortly. The standing variance in Fig. 2b represents 30–40% of the total variance at low frequencies and low wavenumbers. However, recall that the Hayashi technique includes the noise with the propagating variance so that 30–40% may be considered a *lower bound* to the overall contribution of the standing variance to the total variance (not including noise) for wavenumber 2–4 at periods longer than 10 days. In other parts of wavenumber–frequency space, the standing contribution is relatively smaller,

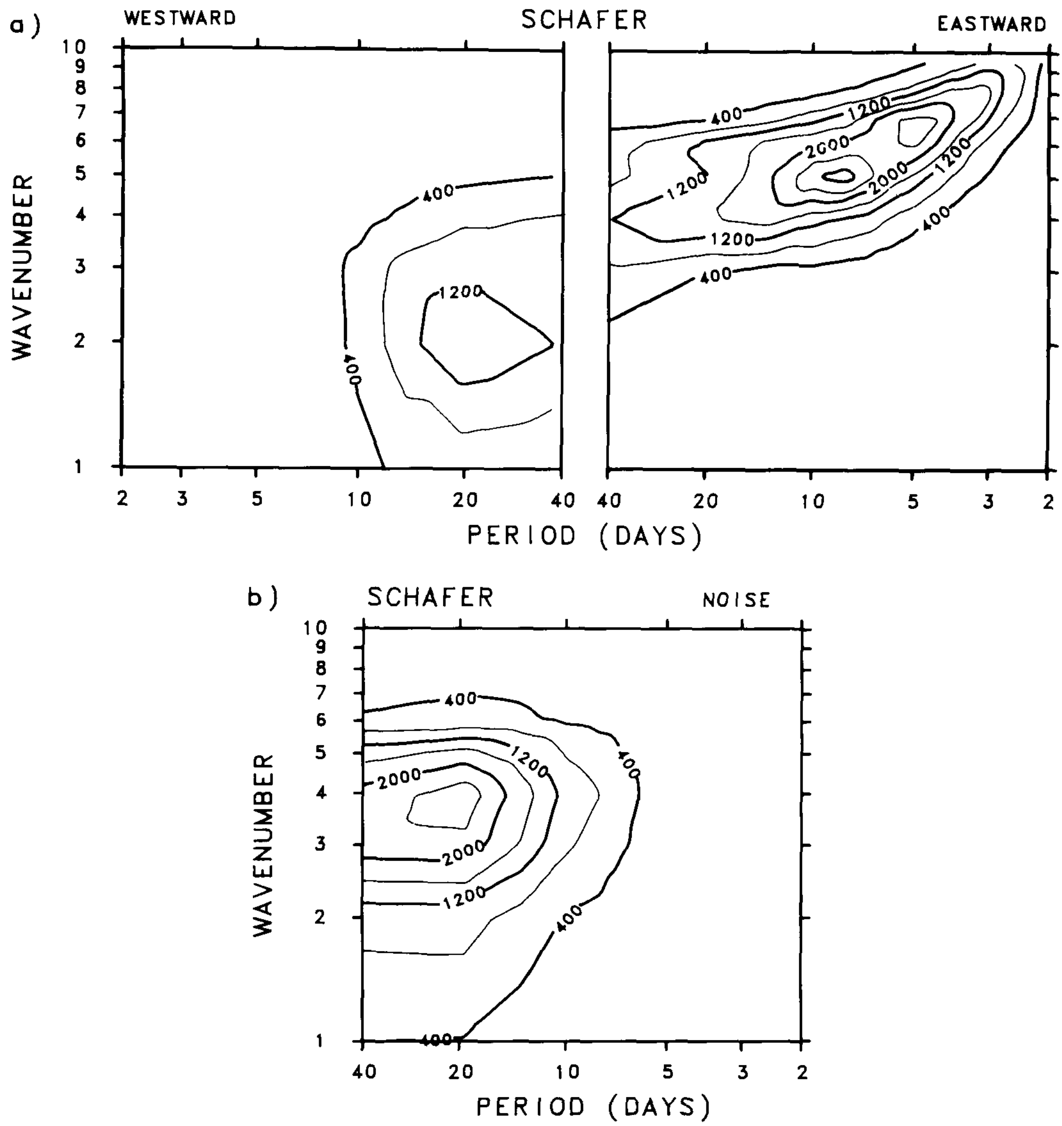

Fig. 3. Power spectral density for the NH winter 500 mb geopotential height averaged between 40° N and 60° N determined by the Schafer method for (a) the traveling variance, and (b) the noise variance. Units are m^2.

although contributions up to 30% of the total occur at the lowest frequencies for wavenumbers 1–5.

Next, consider the power spectra obtained from the Schafer (1979) approach (Fig. 3). The Schafer estimate of the propagating variance (Fig. 3a) is quite similar to that of Hayashi's except at low frequencies where the noise level may have caused an overestimate by Hayashi's technique. The noise (Fig. 3b) is seen to make substantial contributions to the total variance, especially at wavenumbers 3 and 4 and also at wavenumbers 2 and 5, for periods longer than 10 to 20 days. In fact, the noise represents over 50% of the total variance for wavenumbers 3, 4 and 5 at periods longer than 10 days and over 30% at the lowest resolved frequency for all wavenumbers less than 7.

As noted earlier, the Schafer propagating variance estimate includes the contribution of the standing variance. An upper bound on the standing variance can be estimated for this approach at least in terms of order of magnitude by comparing twice the minimum of the coherent eastward and westward propagating variance as discussed earlier. This result is presented in Fig. 4. The greatest power in the upper bound occurs at wavenumbers 3 and 4 for periods longer than 10 days. The fraction of the total *non-noise* variance represented by this upper bound is from 50–75% for wavenumbers 3–5 and periods longer than 10 days. Thus, from a qualitative comparison of the Hayashi and Schafer results, we may conclude that the standing variance represents at least one third and could be as much as 50% to 75% of the total variance in the low-frequency – low-wavenumber part of the spectrum. We have performed a number of experiments using synthetic data with specified spectral content plus red and/or white noise to verify the order of magnitude bounds provided by the techniques as described above.

To verify the existence of the wavenumber 3 standing variance the longitude–time section of the wavenumber 3 height for the winter of 1967–68 is presented in Fig. 5 as an example. Note the fluctuations in time of the wavenumber 3 height while the phase remains predominantly fixed.

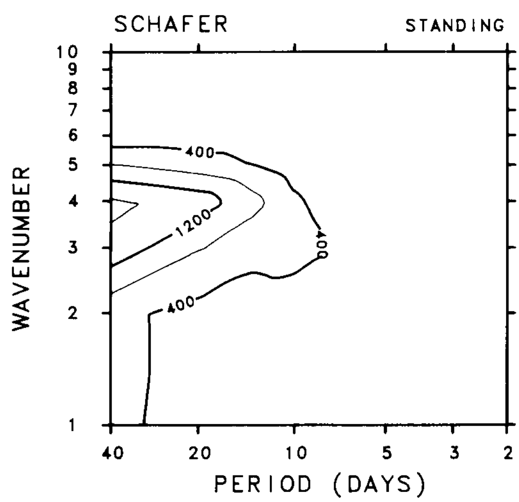

Fig. 4. Upper bound on the NH winter standing variance obtained from the Schafer results. Units are in m^2.

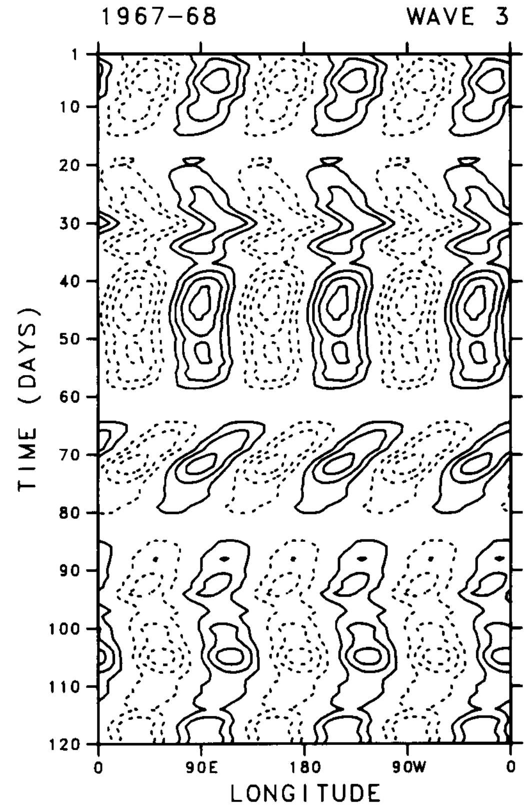

Fig. 5. Longitude-time section of the 500 mb geopotential height of wavenumber 3 for the winter of 1967–68 (day 1 is 16 November and day 120 is 15 March). This diagram illustrates the superposition of stationary, standing and traveling waves of all frequencies for wavenumber 3.

This example is typical of other years as well, and confirms the strong standing variance suggested by power spectral analysis at this wavenumber.

For completeness, the results for the present dataset obtained in the manner of Fraedrich and Böttger (1978) were also computed. The total (one-sided) propagating variance (not shown) is in general agreement with other methods, but the standing variance estimate (Fig. 6) is substantially larger, as noted earlier. However, the resemblance of this estimate to the Schafer noise estimate (Fig. 3b) emphasizes the point that the overestimate is due to the inclusion of the noise in the standing variance estimate for this technique. Nonetheless, the present results indicate that Fraedrich and Böttger's conclusions about the

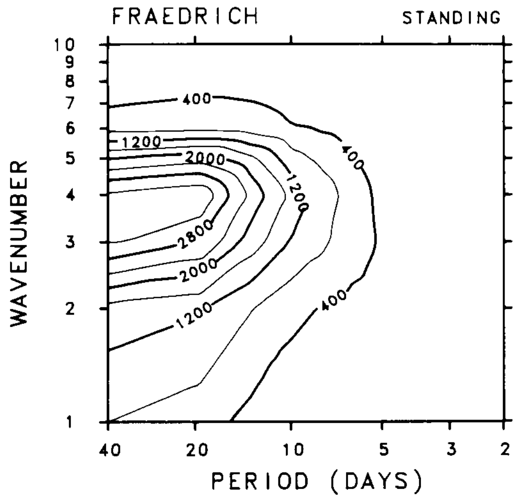

Fig. 6. Power spectral density of the NH winter standing variance determined from the technique used by Fraedrich and Böttger (1978). Units are m^2. Note the similarity to Fig. 3b.

importance of the standing variance, at least in a qualitative sense, are substantially correct.

4.2. Southern hemisphere results

For comparison, it is interesting to briefly consider the corresponding SH behavior. Previous studies of SH power spectra have been presented by Mechoso and Hartman (1982) using FGGE year data and Fraedrich and Kietzig (1983) using South African Weather Bureau data.

The most prominent differences between the hemispheres in terms of traveling variance (Fig. 7) are the much weaker westward propagating variance at ultralong waves in the SH and the extraordinarily strong spectral peak for eastward propagating wavenumber 4 near 13 day period in the SH. These features can also be seen in the sea level pressure power spectra for 1979 discussed by Mechoso and Hartman (1982) as well as in 500 mb data presented by Fraedrich and Kietzig (1983). The value of the wavenumber 4 peak in the SH is a factor of 5 larger than the corresponding value in the NH, which means the SH eastward propagating 13 day wave 4 variance is a factor of 2 to 2.5 larger in amplitude than in the NH. Features similar to the 4 winter mean values in Fig. 7 are also present in each individual winter results (not shown). As in the NH, the Hayashi technique indicates greater low wavenumber traveling variance than Schafer's technique.

The standing variance as estimated by the Hayashi technique in the SH peaks at wavenumber 3. A substantial fraction of the total variance at periods 20 days and longer at wavenumber 3 is attributable to standing fluctuations (Fig. 8a). The standing fluctuations at and near wavenumber 3 in the SH appear to be nearly as intense as those in the NH. Less standing variance is apparent at wavenumbers 2 and 4, however. The upperbound to the standing variance obtained from the Schafer approach (not shown) is quite similar to the Hayashi result. The SH noise level given by Schafer's method shows very large values near wavenumber 3 (Fig. 8b). As in the NH, the standing variance appears to represent a majority of the non-noise variance for wavenumber 3.

Hayashi and Golder (1983) analyzed GCM experiments with and without mountains and found that ultralong-wave westward traveling variance was somewhat decreased in the absence of mountains and that eastward moving wavenumbers 4–6 were markedly increased in the NH in the absence of mountains. Interhemispheric comparison of midlatitude observations from the present and previous studies implies a similar relationship. That is, strong westward propagating ultralong wave variance is present in the NH with its large midlatitude topography, but in the SH with its relatively small midlatitude topography this ultralong wave variance is substantially smaller. Similarly, much stronger eastward traveling variance especially near wavenumbers 4 and 5 is present in the SH compared to the NH. Conversely, fairly strong standing variance is inferred in both hemispheres. Therefore, the rôle of the topography in the general circulation may be more significant for the traveling large-scale waves (wavenumbers $\leqslant 5$) than for the standing waves.

5. Signature of El Niño in midlatitude power spectra

Due to the highly nonlinear character of the general circulation, it may be possible that forcing applied at some particular space and time

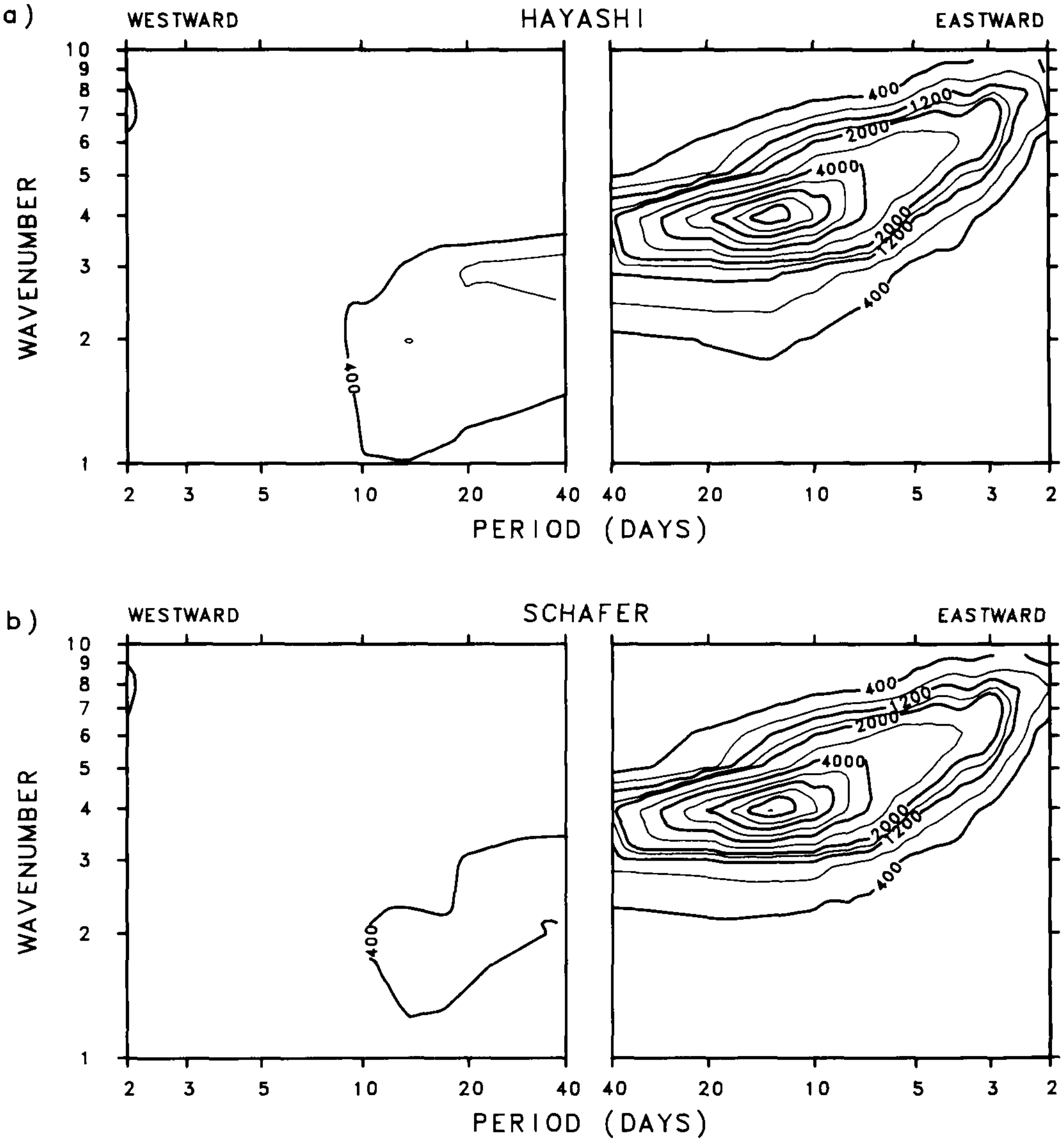

Fig. 7. Power spectral density of the SH winter 500 mb geopotential height averaged between 40°S–60°S for the traveling variance determined by (a) the Hayashi (1979) approach, and (b) the Schafer (1979) approach. Units are m^2. In this figure the contour internal is 400 m^2 up to 2000 m^2 and then 1000 m^2.

scale and at a particular location may induce a response at a remote location at a different space and time scale. This is the fundamental concept behind the teleconnection hypothesis (Bjerknes, 1966, 1969). It is interesting to note that considerable interannual variability can occur in midlatitude power spectra, some of which may be related to external forcing. For example, Mechoso et al. (1987), in the comparison of control and El Niño SST anomaly GCM experiments, found a spectral peak at eastward traveling wavenumber 6 with 4-day period in their anomaly experiment that was absent in the control experiment. They attributed this effect to

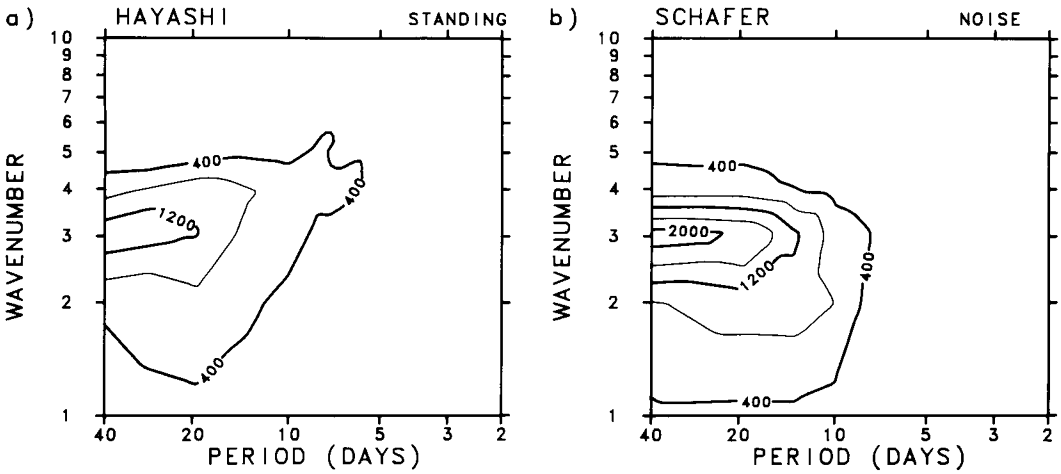

Fig. 8. SH winter power spectra of (a) the Hayashi estimate of the standing variance and (b) the Schafer estimate of the noise variance. Units are m^2.

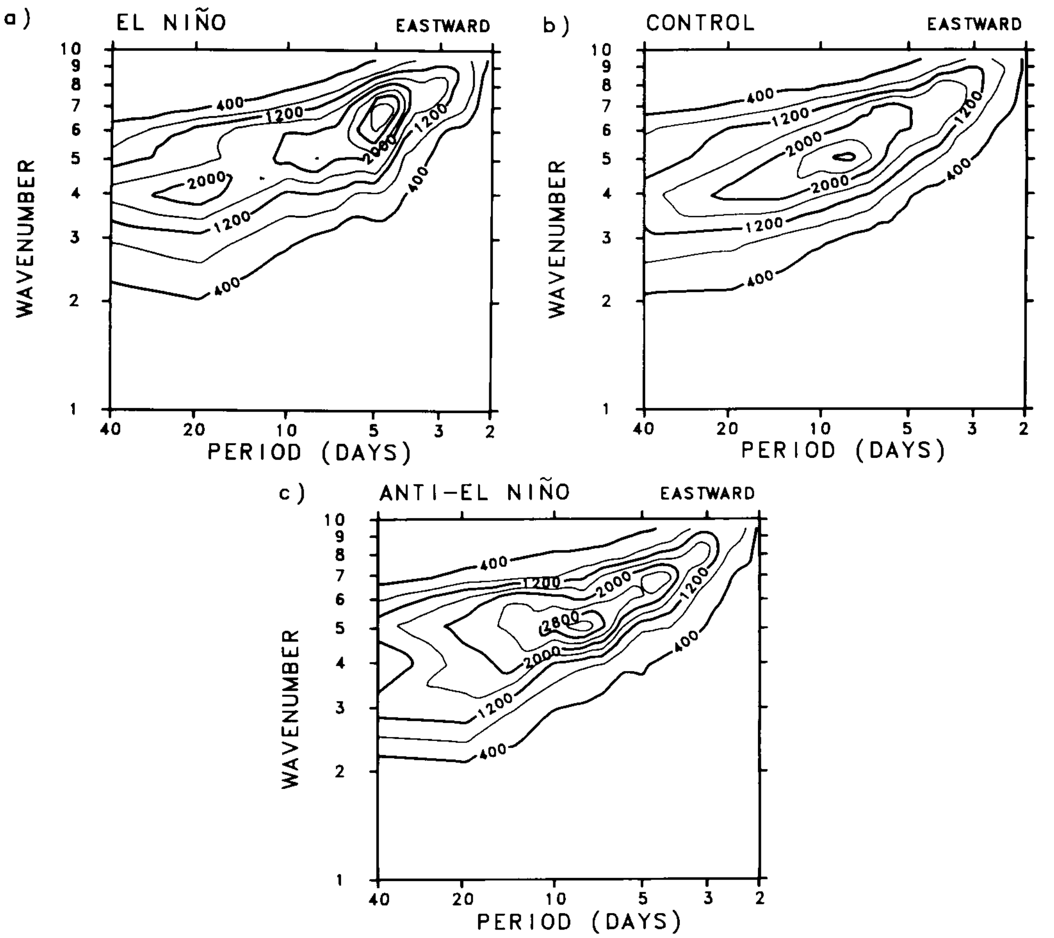

Fig. 9. Power spectral density of the eastward traveling waves for the NH winter 500 mb geopotential height averaged between 40°N and 60°N determined by the Hayashi (1979) technique for (a) the 4 winter El Niño composite, (b) the 9 winter control composite, and (c) the 3 winter anti-El Niño composite. Units are m^2.

an earlier onset of medium scale activity in their simulated El Niño winter compared to the control simulation. Interannual variability can be found in the observed spectral peak of the NH eastward propagating wavenumber 7 at 5-day period shown in Fig. 2a or 3a. To compare with Mechoso et al.'s GCM results, power spectra of 500 mb height averaged from 40°N to 60°N composited from the 4 El Niño winters in the present dataset (1965–66, 1969–70, 1972–73 and 1976–77; Rasmussen and Carpenter, 1982; Livezey and Mo, 1987) are compared to that from 9 control winters which were characterized by neither El Niño nor anti-El Niño (e.g., Held and Kang, 1987) characteristics. These are 1966–67, 1967–68, 1968–69, 1971–72, 1974–75, 1975–76, 1977–78, 1978–79, 1979–80. The El Niño years correspond to warm SST anomalies and the anti-El Niño years to cold SST anomalies in the equatorial Pacific.

The most striking contrast between the two composites is the strong spectral peak at 5-day period for wavenumber 7 in the El Niño composite and its absence in the control composite (Fig. 9), a result similar to that of Mechoso et al.'s GCM experiment. The power in the El Niño peak is over 50% greater than during the control winters. When individual winters are examined (not shown), the 4 El Niño winters all exhibit spectral peaks of varying amplitude near wave 7, 5 day period, the most prominent being in 1972–73 and 1965–66. However, several of the other winters (1967–68, 1968–69, 1971–72, 1973–74, 1975–76) also have peaks in this region of the spectrum. Thus, the wave 7, 5-day period peak is not unique to the El Niño winters.

As an independent test of the hypothesis that El Niño winters exhibit enhanced high frequency eddy activity, the power spectra for the NH winters of 1980–81 through 1983–84 were computed from ECMWF data. The strongest spectral peak near wave 7 at 5-day period in these four winters occurred in 1980–81, not in the El Niño winter of 1982–83. 1982–83 exhibits strongest power in eastward propagating variance in the position of the eastward traveling peak in the composite of the 9 NMC control winters (Fig. 10) with an amplitude more similar to that in the anti-El Niño sample (Fig. 9c). Thus, the possible effect of El Niño on midlatitude high frequency eddies is not clearly evident in all cases.

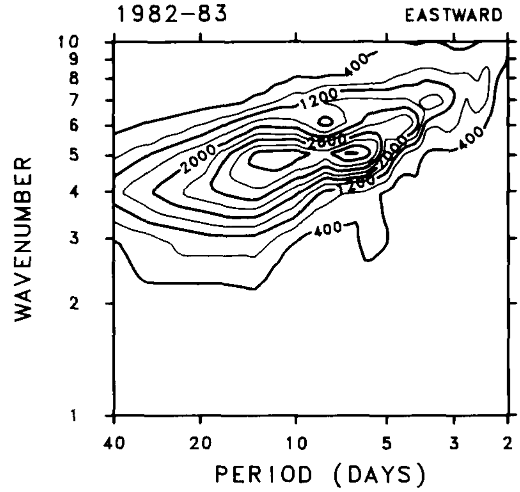

Fig. 10. Power spectral density of the eastward propagating waves for the 1982–83 NH winter 500 mb geopotential height averaged between 40°N and 60°N. Units are m^2.

We also observe that very large interannual variability occurs for westward traveling variance with peak power changing by up to a factor of 4 between extreme winters (not shown). This large interannual variability bears no apparent relationship to the eastern tropical Pacific SST, however, because winters with strong and weak westward traveling variance occur in all of our 3 composites.

Finally, comparing the standing variance for the El Niño, control and anti-El Niño composites revealed a systematic difference. The standing variance in the anti-El Niño composite is up to a factor of 2 greater in much of the spectrum compared to the El Niño composite (Fig. 11). This difference occurs systematically in each of the individual winters in the two composites with the anti-El Niño winters exhibiting consistently strong standing variance. However, the two winters with the strongest standing variance (1966–67 and 1967–68) are found in the control composite whereas the other 7 winters in the control sample are generally similar to the El Niño composite leading to a control composite whose standing variance is midway between the El Niño and anti-El Niño composites.

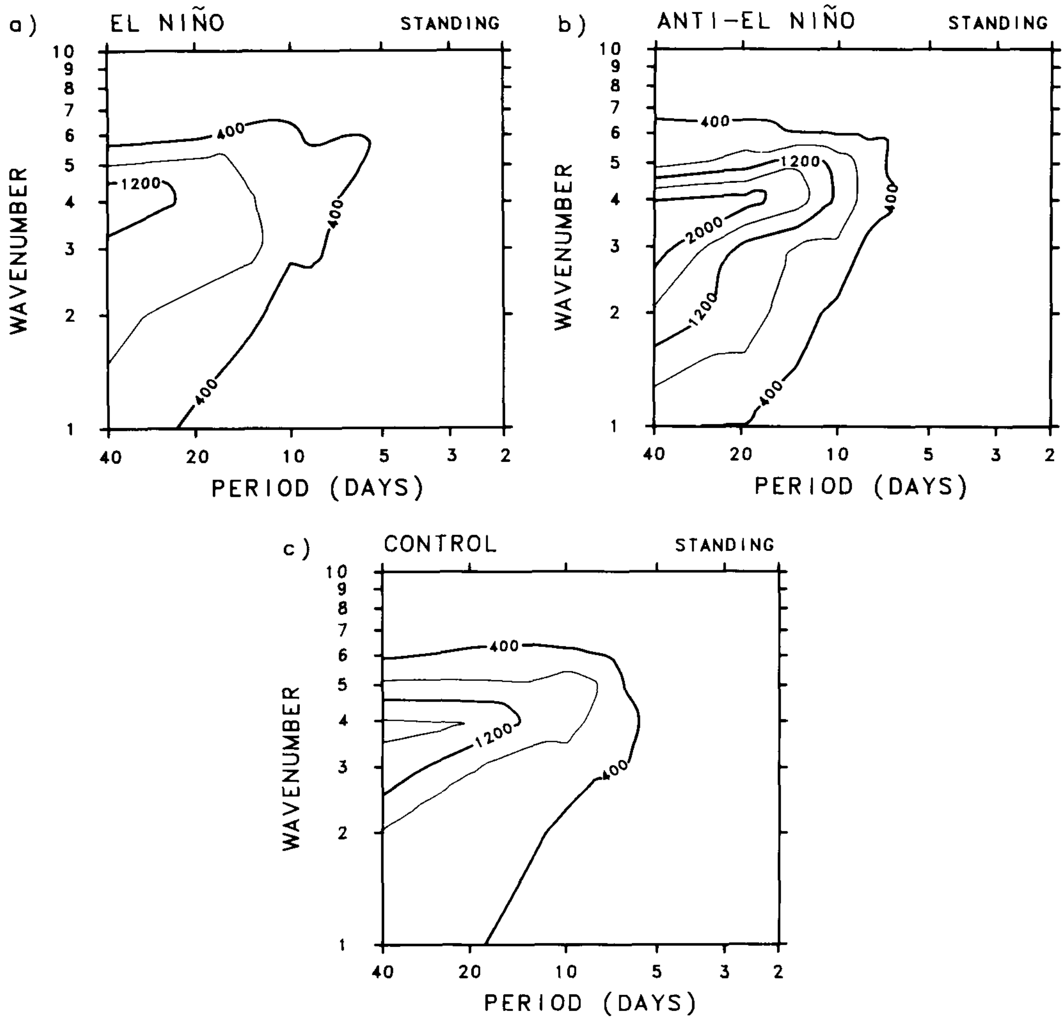

Fig. 11. Power spectral density of the standing variance for the NH winter 500 mb geopotential height averaged between 40°N and 60°N determined by the Hayashi method for (a) the 4 winter El Niño composite, (b) the 3 winter anti-El Niño composite, and (c) the 9 winter control composite. Units are m^2.

6. Summary and conclusion

Three techniques for power spectral analysis developed by Hayashi (1979), Schafer (1979) and Hayashi (1971) were used and compared to explore the level of standing variance in the midlatitude circulation as well as examine interhemispheric differences in the partition of the power spectra. The analysis considered 16 winters of NH data and 4 winters of SH data. Significant standing variance for zonal wavenumbers 2, 3 and 4 at periods 10 to 40 days is indicated in the NH. Strong standing variance at wavenumber 3 is indicated in the SH. It is interesting to note that the regions of the wavenumber spectrum with the largest standing variance correspond to the range of wavenumbers that have been noted to exhibit bimodal amplitude probability density distributions in both hemispheres (Sutera, 1986; Hansen, 1986; Hansen and Sutera, 1986, 1988). The implication is that these two factors are related and that theories of low frequency variability must account for both. The fact that roughly comparable standing variance exists in both hemispheres suggests that the mechanism responsible for this variance is not strongly connected to the stationary forcing provided by topography.

On the other hand, marked differences between the hemispheres in the spectra of the traveling variance are indicated. The NH exhibits much stronger westward traveling ultralong wave variance than the SH while the SH has much stronger eastward traveling variance near wavenumber 4 at 13-day period than does the NH. This result is consistent with earlier studies, and GCM results suggest that the presence in the NH and absence in the SH of strong midlatitude topographic forcing can explain these interhemispheric differences. Thus, topography may play a more important rôle in effecting traveling variance than it does for the standing variance.

In addition, the signature on midlatitude power spectra of the tropical Pacific boundary forcing provided by El Niño and anti-El Niño SST anomalies was investigated. A spectral peak centered at wavenumber 7 at 5-day period is present in the composite El Niño spectrum compared to the composite control spectrum. However, this peak did not occur in the 1982–83 El Niño winter and strong peaks near wavenumber 7 at 5-day period are not unique to El Niño winters. A more systematic difference is observed between the relatively strong standing variance in midlatitudes in the 3 anti-El Niño winters compared to relatively weak standing variance in the El Niño sample. Overall, though, the influence of equatorial Pacific SST anomalies on midlatitude traveling and standing waves is not unequivocal.

7. Acknowledgements

We thank Dr. Y. Hayashi and an anonymous reviewer for their comments which helped to improve the manuscript. This study was supported by the Climate Dynamics Program of the National Science Foundation under grants ATM-8518507 and ATM-8721728 at Control Data. Dr. Sutera was supported under grant ATM-8507496 while at St. Joseph College, West Hartford, CT.

REFERENCES

Benzi, R., Malguzzi, P., Speranza, A. and Sutera, A. 1986a. The statistical properties of general atmospheric circulation: observational evidence and a minimal theory of bimodality. *Q. J. Roy. Met. Soc. 112*, 661–676.

Benzi, R., Speranza, A. and Sutera, A. 1986b. A minimal baroclinic model for the statistical properties of low frequency variability. *J. Atmos. Sci. 43*, 2962–2967.

Bjerknes, J. 1966. A possible response of the atmospheric Hadley circulation to equatorial anomalies of ocean temperature. *Tellus 18*, 820–829.

Bjerknes, J. 1969. Atmospheric teleconnections from the equatorial Pacific. *Mon. Wea. Rev. 97*, 163–172.

Deland, R. J. 1972. On the spectral analysis of traveling waves. *J. Meteor. Soc. Japan 50*, 104–109.

Fraedrich, K. and Böttger, H. 1978. A wavenumber frequency analysis of the 500 mb geopotential at 50°N. *J. Atmos. Sci. 35*, 745–750.

Fraedrich, K. and Kietzig, E. 1983. Statistical analysis and wavenumber-frequency spectra of the 500 mb geopotential along 50°S. *J. Atmos. Sci. 40*, 1037–1045.

Hansen, A. R. 1986. Observational characteristics of atmospheric planetary waves with bimodal amplitude distributions. *Adv. in Geophys. 29*, 101–133.

Hansen, A. R. and Sutera, A. 1986. On the probability density distribution of the planetary-scale atmospheric wave amplitude. *J. Atmos. Sci. 43*, 3250–3265.

Hansen, A. R. and Sutera, A. 1988. Planetary wave amplitude bimodality in the Southern Hemisphere. *J. Atmos. Sci. 45*, 3771–3783.

Hayashi, Y. 1971. A generalized method of resolving disturbances into progressive and retrogressive waves by space Fourier and time cross-spectral analysis. *J. Meteor. Soc. Japan 49*, 125–128.

Hayashi, Y. 1977. On the coherence between progressive and retrogressive waves and a partition of space–time power spectra into standing and traveling parts. *J. Appl. Meteor. 16*, 368–373.

Hayashi, Y. 1979. A generalized method of resolving transient disturbances into standing and traveling waves by space–time spectral analysis. *J. Atmos. Sci. 36*, 1017–1029.

Hayashi, Y. 1982. Space–time spectral analysis and its applications to atmospheric waves. *J. Meteor. Soc. Japan 60*, 156–171.

Hayashi, Y. and Golder, D. G. 1977. Space–time spectral analysis of mid-latitude disturbances appearing in a GFDL general circulation model. *J. Atmos. Sci. 34*, 237–262.

Hayashi, Y. and Golder, D. G. 1983. Transient planetary waves simulated by GFDL spectral general circulation models. Part I: Effects of mountains. *J. Atmos. Sci. 40*, 941–950.

Held, I. M. and Kang, I.-S. 1987. Barotropic models of the extratropical response to El Niño. *J. Atmos. Sci. 44*, 3576–3586.

Livezey, R. E. and Mo, K. C. 1987. Tropical-extratropical teleconnections during the Nothern Hemisphere winter. Part II: Relationships between monthly mean Northern Hemisphere circulation patterns and proxies for tropical convection. *Mon. Wea. Rev. 115*, 3115–3131.

Lorenz, E. N. 1967. *The nature and theory of the general circulation of the atmosphere*. WMO Publication 218, T.P. 115, World Meteorological Organization, Geneva, Switzerland, 161 pp.

Mechoso, C. R. and Hartman, D. L. 1982. An observational study of traveling planetary waves in the Southern Hemisphere. *J. Atmos. Sci. 39*, 1921–1935.

Mechoso, C. R., Kitoh, A., Morrthi, S. and Arakawa, A. 1987. Numerical simulations of the atmospheric response to a sea surface temperature anomaly over the equatorial eastern Pacific ocean. *Mon. Wea. Rev. 115*, 2936–2956.

Pratt, R. W. 1976. The interpretation of space–time spectral quantities. *J. Atmos. Sci. 33*, 1060–1066.

Pratt, R. W. and Wallace, J. M. 1976. Zonal propagation characteristics of large-scale fluctuations in the mid-latitude troposphere. *J. Atmos. Sci. 33*, 1184–1194.

Rasmussen, E. M. and Carpenter, T. H. 1982. Variations in tropical sea surface temperature and surface wind fields associated with the Southern Oscillation/El Niño. *Mon. Wea. Rev. 110*, 354–384.

Schafer, J. 1979. A space–time analysis of tropospheric planetary waves in the Northern Hemisphere. *J. Atmos. Sci. 36*, 1117–1123.

Speth, P. and Madden, R. A. 1983. Space–time spectral analyses of Northern Hemisphere geopotential heights. *J. Atmos. Sci. 40*, 1086–1100.

Sutera, A. 1986. Probability density distribution of large-scale atmospheric flow. *Adv. in Geophys. 29*, 227–249.

Tsay, C. Y. 1974. A note on the methods of analyzing traveling waves. *Tellus 26*, 412–415.

Wallace, J. M. and Blackmon, M. L. 1983. Observations of low-frequency atmospheric variability. In: *Large-scale dynamical processes in the atmosphere* (eds. B. Hoskins and R. Pearce). New York: Academic Press, 55–94.